JOURNAL OF MATERIALS SCIENCE 7 (1972) 265-278

Transmission Electron Microscope Observations on GaP Electroluminescent Diode Materials

B. D. CHASE*, D. B. HOLT
Metallurgy Department, Imperial College, London, SW7, UK

Transmission electron microscope observations were made on GaP material grown by liquid epitaxy, vapour phase epitaxy and Czochralski pulling from the melt. The vapour phase material was found to contain many intrinsic stacking faults. Most were linear but a few were tetrahedral. Both Frank and Shockley partial dislocations were found. The fault density increased with increase in the Te dopant concentration in the vapour phase material. The Czochralski material also contained intrinsic stacking faults, and its defect content was higher than that of layers grown by liquid phase epitaxy. In all specimens with free carrier concentrations greater than 10^{18} cm^{-3} evidence was found to suggest that precipitation of impurities had taken place.

1. Introduction

GaP red electroluminescent diodes with external quantum efficiencies greater than 3% can be produced with a high yield using a process of double liquid epitaxy whereby suitably doped n- and p-type layers are consecutively grown on to a GaP substrate [1]. Diodes grown using pulled (Czochralski grown) or vapour phase grown material adjacent to the active region are found to give relatively low performances with external quantum efficiencies in general less than 0·1% [2]. The reasons for this are not yet fully understood.

It had been found useful in the case of GaAs lasers to employ a range of techniques for the analysis of structure in relation to device performance [3, 4]. The present work forms part of a similar survey of the types of structural inhomogeneity found in GaP lamps (electroluminescent diodes) and lamp materials. This paper presents the results of an investigation undertaken using transmission electron microscopy. GaP diode material grown by each of the three basic processes mentioned above and with a range of dopants and doping levels was examined. Results obtained using scanning electron microscopy will be reported separately [5].

Transmission electron microscopy has been applied extensively to the study of defects in silicon and germanium [6, 7]. In the case of III-V compounds studies have been limited in the main to GaAs [3, 8-11] with some attention being given to GaP grown from the vapour phase [12] or pulled from the melt [13]. Hitherto, however, no transmission electron microscope observations on liquid epitaxy grown GaP have been published.

Considerable effort has been directed to the development of GaP as a material for the production of electroluminescent devices but few observations have been made on structural defects in this material. Optical microscopy, etching and X-ray topography have provided some information but these techniques are of limited resolving power. In the present work a transmission electron microscope analysis was made of the defects present in a range of samples. It was found that the highest defect concentrations existed in material grown by vapour phase epitaxy and that these concentrations increased with doping level.

2. Experimental Methods

GaP was prepared for transmission electron microscopy by a modification of a technique

*Present address: – IBM Manufacturing Research Laboratory, Hursley Park, Winchester.
This work was carried out at the Department of Metallurgy, Imperial College, London, SW7, UK.

© 1972 Chapman and Hall Ltd.

originally developed for GaAs [14]. A photomultiplier detected the transmission of blue light to which thick GaP is opaque. Significant transmission occurred when the specimen was thin enough for transmission electron microscopy and the photomultiplier signal was employed to trigger the removal of the specimen from the reagent jet.

All specimens were of {111} orientation and for thinning from the P($\bar{1}\bar{1}\bar{1}$) face a chemical reagent consisting of chlorine gas dissolved in methanol was found satisfactory [15]. Thinning from the Ga (111) face was effected using the same reagent but with the specimen anodically biased to a potential of between 100 and 240 V with respect to an electrode positioned within the jet. A more complete account of the thinning technique and of the electrochemical tunnel etching which could be produced will be published elsewhere [16, 17].

All the GaP material examined in this paper was produced at the Services Electronic Research Laboratories at Baldock and kindly supplied by them. The GaP crystals were grown either from a stoichiometric melt [18], by liquid phase epitaxy [1] or by vapour phase epitaxy [19]. Specimens produced by each of these techniques were examined. Large single crystals were pulled from the melt using the liquid encapsulation technique [18]. Liquid phase epitaxy of GaP was carried out using both the tipping and vertical dip methods. Diodes were fabricated by growing n-type (Te or S doped) layers on to the P($\bar{1}\bar{1}\bar{1}$) faces of pulled substrates. This was followed by the overgrowth of a p-type (Zn and O doped) material. To examine this p-type layer it was thus necessary to remove the substrate and n-type layer by thinning from the Ga (111) face. To make this possible the electrochemical thinning process was developed and this produced thin areas with a good surface finish [16, 17]. Vapour phase material was deposited on to the Ga (111) faces of GaAs substrates using a PCl_3, H_2 vapour transport system. In this case chemical means alone sufficed to remove the GaAs layer and to thin the GaP from the P($\bar{1}\bar{1}\bar{1}$) face.

3. Results

As the method of growth is relevant to the interpretation of the micrographs the results are presented separately for each class of material.

The micrographs unless otherwise stated were taken using a two beam condition with a single operating diffraction vector. Kikuchi lines were present in the diffraction patterns from all specimens and enabled two beam conditions to be selected with a high degree of precision.

3.1. GaP grown by Vapour Phase Epitaxy

The specimens examined are listed in table I.

TABLE I Vapour phase epitaxy specimens examined in the transmission electron microscope. All the specimens were doped with Te and are arranged in increasing order of free electron concentration.

Specimen (SERL No.)	Free electron concentration cm^{-3}
AP 64/2	Intrinsic
VP 571/2	6×10^{16}
VP 574/3	1×10^{17}
AP 118/2	10^{17} to 10^{18} estimate
AP 133/4	$2{\cdot}2 \times 10^{17}$
AP 143/2	$2{\cdot}2 \times 10^{17}$
AP 136/7	$1{\cdot}1 \times 10^{18}$

All specimens were doped with Te. Difficulty was experienced in chemically jet thinning specimens with low free electron concentrations. There was a tendency for a rough rather than a polished surface to form at the bottom of the

Figure 1 Tetrahedral stacking faults in vapour phase grown GaP. (a) Bright field image.

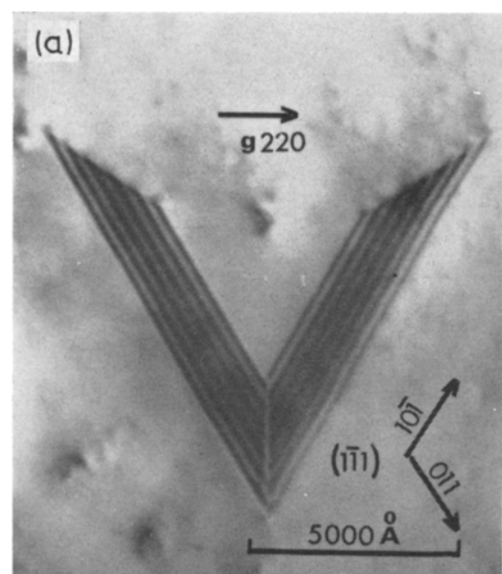

Figure 1a

dimple. From the electron micrographs of specimen VP 571/2 it was evident that preferential attack had occurred at certain planar defects. No additional diffraction spots were visible in selected area diffraction patterns from these defects. This would be consistent with the defects being stacking faults rather than twins. However, preferential thinning of the foil at twins could make the detection of twinned material impossible. In addition the large degree of inelastic scattering, as evidenced by the predominance of the Kikuchi lines observed

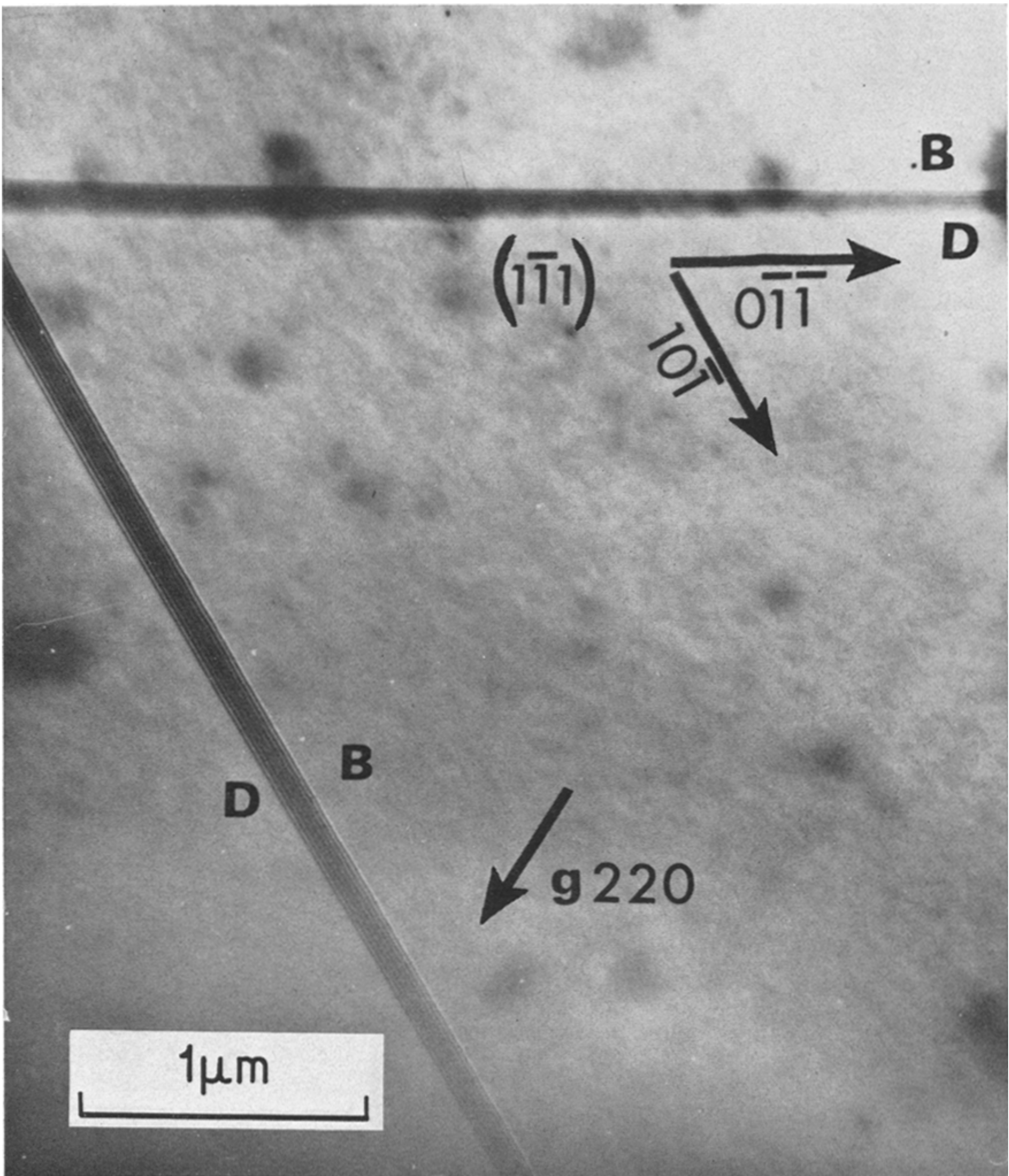

Figure 1(b) Dark field image. The [220] diffraction vector points towards the dark fringe therefore the fault is intrinsic.

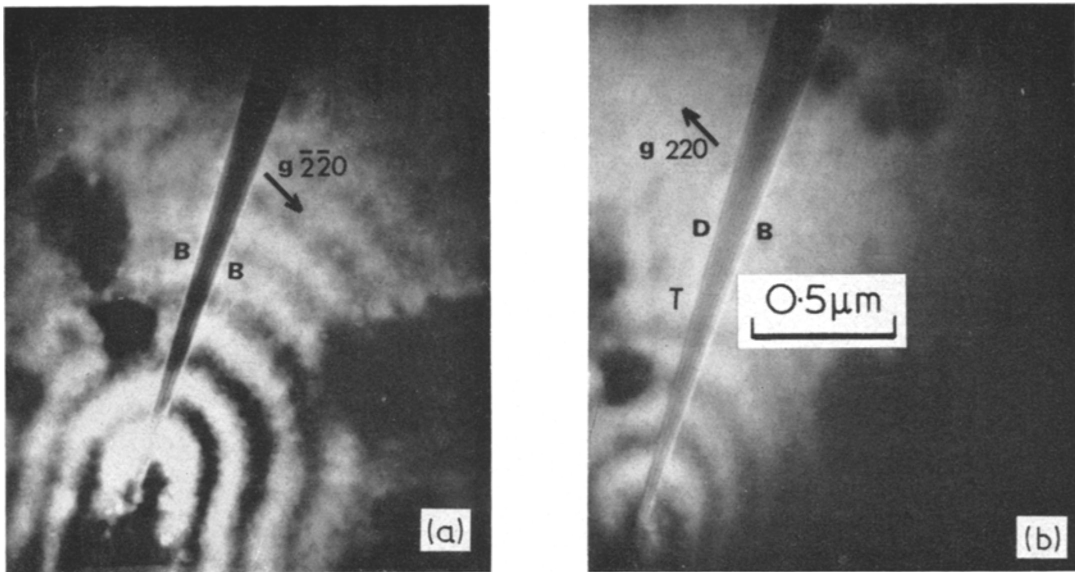

Figure 2 (a) Bright field and (b) dark field image of a linear stacking fault in vapour phase grown GaP. In the dark field image the [220] diffraction vector **g** points towards the dark fringe therefore the fault is intrinsic. Due to the reversal of **g** between the two micrographs the top edge of the fault, marked T, shows fringes of different contrast in the two micrographs.

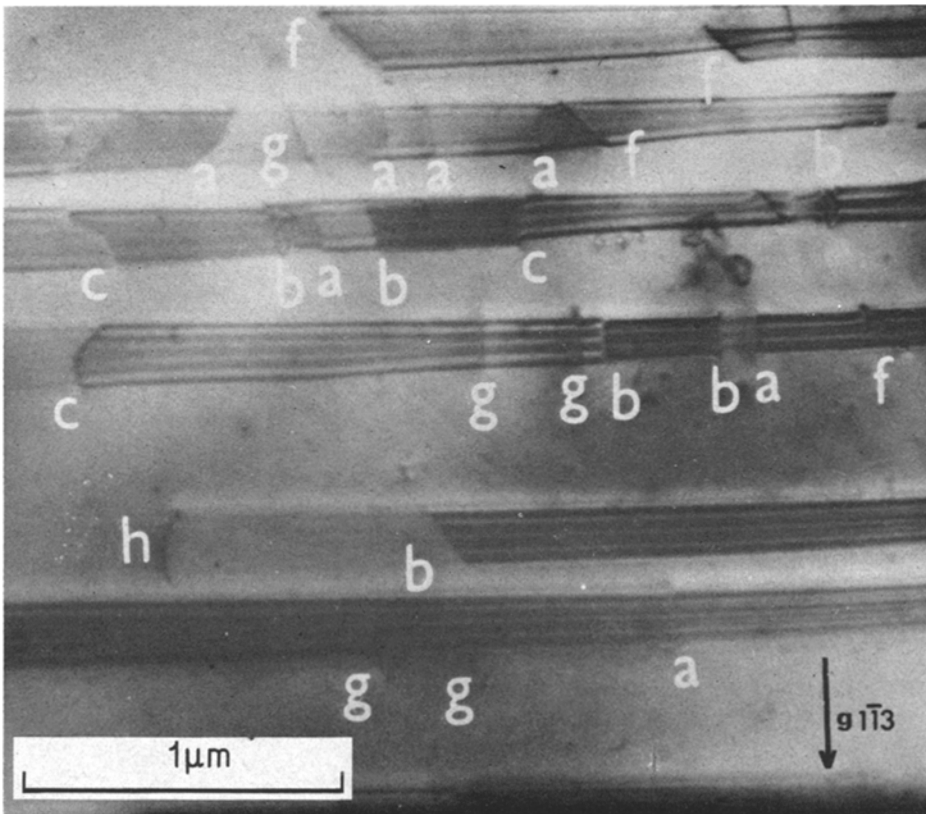

Figure 3a

in the diffraction pattern, means that any additional reflections would have to be of high intensity to be visible.

The more highly doped specimens with carrier concentration $N > 2 \times 10^{17}$ cm^{-3} were easier to thin and no preferential etching at defects was observed. The most common defects were identified as stacking faults. The majority of these were linear in nature but in some specimens tetrahedral faults were also observed (fig. 1). Bright field and dark field micrographs of a linear stacking fault are shown in fig. 2. Analysis of these showed that the faults were intrinsic in nature. For such purposes care was taken to choose a single fault rather than a series of overlapping faults which would give ambiguous results. It was established that tetrahedral faults such as shown in fig. 1 were also intrinsic. The method used for the analysis was that described by Amelinckx [20]. If the reflection is of the type 400, 220 or 111, and if the diffraction vector with its origin at the centre of the fault points towards the dark fringe in the dark field image, the fault is intrinsic as in figs. 1b and 2. The reverse is true for reflections of type 200 and 222.

More complex stacking faults were found in specimen AP 118/2. An analysis was made of the Burgers vectors of the dislocations associated with the faults shown in fig. 3. The plane of the foil was close to a $\{111\}$ orientation and was arbitrarily assigned the indices $(\bar{1}11)$. The faults gave no fringe contrast when observed in bright field using the 220 reflection (fig. 3b). For this to occur $\mathbf{R} \cdot \mathbf{g} = 0$ (Hirsch *et al* [21]), and thus the fault displacement vector $\mathbf{R}$ can only be of type $\pm \frac{1}{3} \mid 1\bar{1}1 \mid$ or $\pm \frac{1}{3} \mid 1\bar{1}\bar{1} \mid$.

Figure 3 Bright field micrographs of a stacking fault complex in vapour phase grown GaP slice no. AP136/7, Te doped to a free carrier concentration 1×10^{18} cm^{-3}. These micrographs were taken with the operative reflections, **g**, marked.

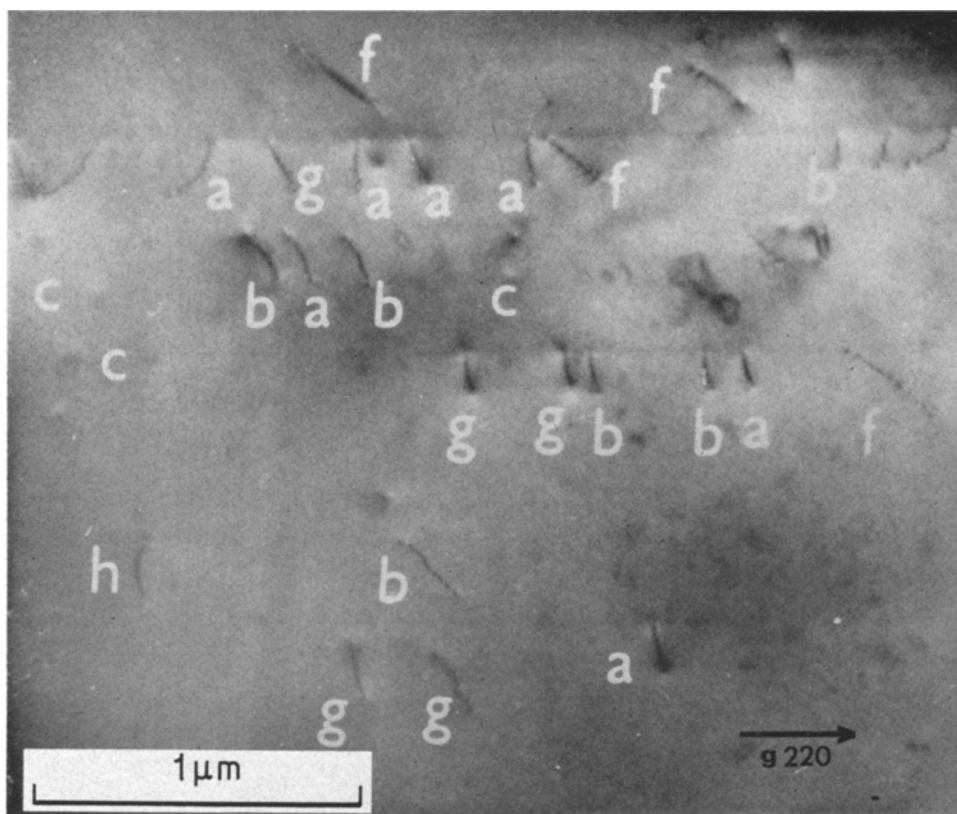

Figure 3b

When the faults were observed using the 202 reflection, fringes were visible, i.e. $\mathbf{R} \cdot \mathbf{g} \neq 0$. Only the value $\mathbf{R} = \pm \frac{1}{3} \mid 1\bar{1}1 \mid$ is consistent with both observations and therefore the faults lie in the $(1\bar{1}1)$ plane.

The terminology and diffraction contrast theory relating to stacking faults in fcc materials can be applied directly to the sphalerite structure since the sphalerite structure has an fcc space lattice, with a basis unit of two atoms. The atomic arrangement in stacking faults in the diamond structure was discussed by Hornstra [22] using ball and wire crystal models. Holt [23] extended this treatment to the sphalerite structure and pointed out that there was a geometrical possibility of two types of fault in this structure. These two types are upright and inverted. The latter type has a high energy structure with bonds between like atoms occurring both above and below the fault plane. In the present work the observed contrast effects could be explained in terms of faults with the expected $\mathbf{R}$ vectors for a structure with the fcc space lattice. It is unlikely that upright and inverted faults would produce distinguishably different contrast effects. The fringe contrast exhibited by a stacking fault results essentially from differences in the phase angle of electrons scattered in material above and below the fault plane. Any additional contrast effects due to alterative atomic arrangements within the fault would be very weak because only a layer two atoms thick is involved. Hence it is not to be expected that the upright or inverted character of faults can be determined by diffraction contrast observations.

The Burgers vectors of the partial dislocations associated with the faults of fig. 3 were determined using the invisibility criteria as described by Silcock and Tunstall [24]. A table was made out to show the value of $\mathbf{g} \cdot \mathbf{b}$ for possible dislocations in the $(1\bar{1}1)$ plane, (table II). For a perfect screw dislocation the invisibility criterion is that $\mathbf{g} \cdot \mathbf{b} = 0$; the presence of an edge component can however make the dislocation visible even under these conditions. For a Shockley type partial dislocation with no edge component the invisibility criterion is that $\mathbf{g} \cdot \mathbf{b} = \pm \frac{1}{3}$. For values $\mathbf{g} \cdot \mathbf{b} = \pm \frac{2}{3}, \pm \frac{4}{3}$ the dislocation will be visible. When an edge component is present, the dislocation will only be invisible when $\mathbf{g} \cdot \mathbf{b} = \pm \frac{1}{3}$ if the value $\xi\mathbf{g}\ S\mathbf{g}$ is small. Here $\xi\mathbf{g}$ is the extinction distance and $S\mathbf{g}$ is the distance in reciprocal space of the reciprocal lattice point from the sphere of reflection measured parallel to the beam (see Amelinckx [20], p. 126). For a Frank partial, which is an edge dislocation, the invisibility criterion is less well-defined. Even when $\mathbf{g} \cdot \mathbf{b} = 0$ the dislocation can still be intensely visible due to the finite value of $\mathbf{g} \cdot \mathbf{b} \times \mathbf{u}$, where $\mathbf{u}$ is the unit vector in the dislocation line. Invisibility can only be expected for the case where $\mathbf{g} \cdot \mathbf{b} \times \mathbf{u} = 0$. This condition takes account of the lattice displacement characteristic of an edge dislocation and has been treated theoretically by Howie and Whelan [25]. As a result of this, the Frank partial with $\mathbf{b} = \frac{1}{3}\ [1\bar{1}1]$ can be visible in the 220 reflection even though $\mathbf{g} \cdot \mathbf{b} = 0$.

In order to perform a valid analysis of Shockley partial dislocations it was necessary to determine the experimental limits of the value of $\xi\mathbf{g}\ S\mathbf{g}$. According to Silcock and Tunstall [24] the criterion for unambiguous results is that $\xi\mathbf{g}\ S\mathbf{g}$ should be less than about 0·3.

To calculate $\xi\mathbf{g}$ the expression

$$\xi\mathbf{g} = V \cos \theta / \lambda\, F\mathbf{g}\,.$$

was used (Hirsch *et al* [21], page 102). Here V is the volume of the unit cell, λ the wavelength of the electrons, $F\mathbf{g}$ the structure factor and θ the Bragg angle. The structure factor was calculated using the expression

$$\mid F\mathbf{g} \mid^2 = 16[f_{\mathrm{Ga}}{}^2 + f_{\mathrm{P}}{}^2 + 2f_{\mathrm{Ga}}\, f_{\mathrm{P}} \cos \pi/2\ (h + k + l)]$$

(Cullity [26]. The atomic scattering amplitudes for electrons f_{Ga} and f_{P} were taken from tables given by Hirsch *et al* and were relativistically corrected for 100 kV electrons. For this purpose the relevant parameter $(\sin \theta)/\lambda$ was calculated using the Bragg equation $\lambda = 2d \sin \theta$. The wavelength of 100 kV electrons was taken as 0·037 Å and the lattice parameter of GaP as 5·4505 Å [27]. The calculated extinction distances for the relevant reflections are given in table III. The accuracy of the calculated values of $\xi\mathbf{g}$ is limited by uncertainty in the scattering amplitudes which are not known to better than a few per cent. Other possible errors involved in the calculation are discussed by Hirsch *et al.* The calculated values can be judged correct only to within about $\pm$ 10%.

The value of $S\mathbf{g}$ can be determined by observa-

TABLE II Values of **g** . **b** for dislocations lying in the $(1\bar{1}1)$ plane.

Reflection	b	1/6 $[21\bar{1}]$	1/6 [112]	1/6 $[\bar{1}12]$	1/3 $[1\bar{1}1]$	½ [110]	½ $[10\bar{1}]$	½ [011]
[202]		1/3	2/3	2/3	4/3	1	0	1
[220]		1	1	0	0	2	1	1
[422]		4/3	5/3	1/3	4/3	1	1	1
$[\bar{2}\bar{4}2]$		−5/3	−4/3	1/3	4/3	1	1	1
$[1\bar{1}3]$		−1/3	1/3	2/3	5/3	0	−1	1

For Shockley partials (**b** = 1/6 < 112 >) invisibility will occur only where **g** . **b** = 0 or ± 1/3. Total dislocations of screw nature (**b** = ½ < 110 >) will be invisible only when **g** . **b** = 0. The Frank partial (**b** = 1/3 $[1\bar{1}1]$) possesses strong edge character (see text) and will be visible even for the case **g** . **b** = 0.

TABLE III Calculated values of ξg for various reflections and values of $\Delta x/x$ for ξ**g** **Sg** = 0·3.

Reflection	$\frac{\sin\theta}{\lambda}$ Å^{-1}	f_{Ga} Å	f_{P}Å	F_{g}Å	ξg Å	$\frac{\Delta x}{x}$
[220]	0·26	3·48	2·48	23·8	577	0·053
[113]	0·30	3·03	2·04	14·6	941	0·024
[224]	0·45	2·04	1·15	12·8	1072	0·01

tion of the Kikuchi line pattern (Amelinckx [20], page 125). When Δx is the displacement on the plate of the Kikuchi line in relation to the diffraction spot and x is the distance of the spot from the centre of the pattern:

$$Sg = \Delta x\lambda/xd^2_{\text{hkl}}$$

For each reflection this expression was used to calculate values of $\Delta x/x$ which would satisfy the condition $\xi g\ Sg = 0{\cdot}3$; these are listed in the table. It is apparent that as the reflections increase in order it becomes more difficult to align the specimen within the critical condition. In practice it was found that for the 220 and $1\bar{1}3$ reflections an adequate degree of accuracy was achieved.

For the higher order reflections of type 422 it was found that the maxima of the two spots occurred at slightly different angles of tilt. This made exact alignment very difficult and measurements on the diffraction patterns gave values for $\Delta x/x$ greater than 0·5 and outside the acceptable limits. As sufficient information was available from the lower order reflections for dislocation analysis the 422 reflections were not used.

A check that $\xi g\ Sg < 1$ can be simply made by observation of the fringes in the stacking fault. Whelan and Hirsch [28] showed that when $\xi g\ Sg < 0{\cdot}5$, dynamical conditions of diffraction result in each stacking fault fringe having a double minimum. This can be seen clearly in fig. 3a where each fringe appears as a double dark line.

The observed visibilities of a large number of dislocations in different reflections were compared with the predicted visibilities in table II. It was found that the majority of dislocations were Shockley partials with a Burgers vector of type **b** = $a/6$ $[21\bar{1}]$. These are denoted by the letter "a" on the micrographs. All the dislocations so marked in fig. 3 were visible in the 220 reflection and were either invisible or exhibited very faint contrast in the 202 and $1\bar{1}3$ reflections which is consistent with the predictions of table II. Similarly those of type **b** = $a/6$ [121] and **b** = $a/6$ $[\bar{1}12]$ are denoted by the letters "b" and "c" respectively.

Some dislocations were found which were visible in all reflections. Comparison with the table indicates that these will either be perfect dislocations or else Frank partials. A Frank partial must bound a region of stacking fault and, even in a system of overlapping faults such as that here, can be distinguished from a perfect dislocation by the change in nature of the fault fringes either side. Frank partials with **b** = $a/3$ $[1\bar{1}1]$ and exhibiting the above contrast are denoted by the letter "f". Perfect dislocations with no associated change in fringe contrast are denoted by the letter "g" but there was insufficient data for Burgers vector determination. The dislocation at "h" was visible in all reflections and gave the appearance of terminating a stacking fault. The stacking fault immediately adjacent gave only very faint fringe contrast so no unambiguous analysis could be made.

Certain dislocations were found to have well defined line directions. In particular all the Frank partials lay along the $[10\bar{1}]$ direction. The Shockley partials were found to lie variously along the [011], $[\bar{2}13]$, $[1\bar{1}2]$ and $[1\bar{2}3]$ directions with no particular correlation between the

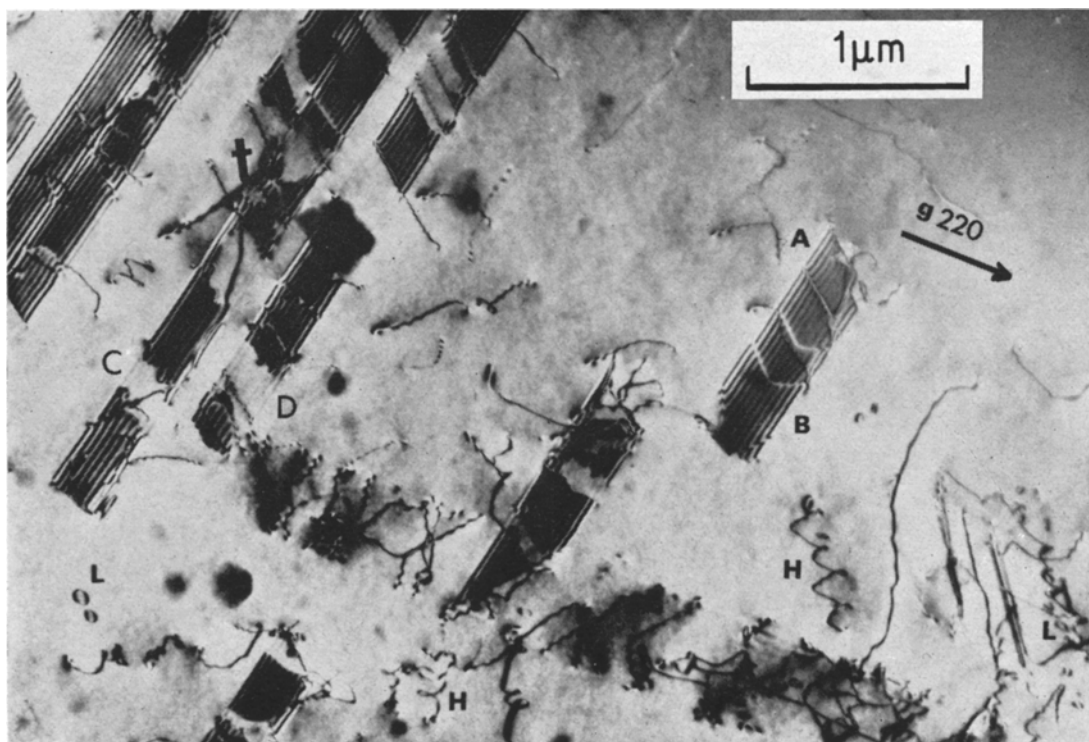

Figure 4 Dark field micrographs showing defects in vapour phase grown specimen AP136/7. Helical dislocations are marked H and loops L.

direction and the assigned Burgers vector, and a large number of the Shockley partials were bowed.

The most complex defect structure was found in specimen no. AP 136/7 which also had the highest doping level. Fig. 4 is a dark field micrograph illustrating some of these defects. The plane of the foil was found to be close to {114}. Two sets of stacking faults are present but one set lying parallel to the [$\bar{2}$20] direction is out of contrast. It can be seen that the apparent nature, intrinsic or extrinsic, of the stacking faults varies along their length. For example at A the position of the bright fringe indicates an intrinsic fault whereas that at B indicates an extrinsic fault. This is interpreted as a case of faults on adjacent planes overlapping one another. Whelan and Hirsch [28] showed that the fringe contrast of a stacking fault is governed by the phase angle $\alpha = 2\pi\mathbf{g} \cdot \mathbf{R}$ where $\mathbf{R}$ is the displacement vector of the fault. If $\alpha = +2\pi/3$, a single fault in bright field will show bright edge fringes and it will show dark edge fringes for $\alpha = -2\pi/3$. If two intrinsic faults overlap one another on closely adjacent planes the total phase angle is simply the sum of the individual phase angles. If α is $2\pi/3$ for each fault individually it is $4\pi/3$ for the pair; this is equivalent to $-2\pi/3$. Thus α changes sign and the fringes from the pair reverse in the sense that light fringes become dark fringes and vice versa. This applies equally in dark field so that the pair together is equivalent to an extrinsic fault. For three overlapping faults $\alpha = 6\pi/3$ which is equivalent to $\alpha = 0$ and no fault contrast would be expected. In practice a finite spacing between fault planes results in faint fringes appearing as at C and D in fig. 4.

Also visible in the micrograph are a number of helical dislocations H and dislocation loops L. Stereo pair analysis was used to show that the helices were in fact helical dislocations and not just a series of dislocation dipoles.

Other interesting defects were found in a different region of the same specimen. Fig. 5a shows a dislocation complex associated with a subgrain boundary. The tilt across the boundary could be detected in the electron microscope

by a small rotation of the selected area diffraction pattern as the boundary was traversed. Of interest are the different types of interface which were shown by trace analysis to be of types (1 1 1), (1 $\bar{1}$ $\bar{1}$) and (1 2 2) when the normal to the foil had the indices [1 1 4]. A good example of a cross slip loop marked L is seen on the (1 2 2) plane. The dark lamellae also visible in the micrograph gave extra spots in selected area diffraction. This identified the lamellae as microtwins as distinct from stacking faults which would not give rise to extra spots. The finite width of these features which lie in the (1 1 1) plane can be observed by comparison with the projected image of one of the associated dislocations. Another example of a microtwin is seen in fig. 5b. Here characteristic wedge fringe contrast can be observed at the edges even though a multibeam diffraction condition was operating. Fig. 6a is bright field image illustrating a stacking fault complex of a slightly different nature to those of fig. 4. Two main overlapping fault lines are visible. The upper one in the micrograph (lettered a to i) exhibits distinct sections showing a number of different types of fault contrast. This is clearly characteristic of a number of overlapping faults on closely adjacent planes. On the other hand the lower fault line (lettered j to u) exhibits only two types of fringe contrast. In the one, fringes are clearly visible whilst in the other the fringes are very faint. The suggested explanation for this contrast is that a number of total dislocations have moved into an atomic plane or planes close to an original fault system. These dislocations have subsequently dissociated to give a number of small regions of stacking fault bounded by partial dislocations. Examination of the lower edge of the fault at point j in the micrograph indicates that the original system may have consisted of a pair of overlapping intrinsic faults so that, for the two, $\alpha = 4\pi/3$. The dissociation of a total dislocation to give a further region of intrinsic fault would give a sum total of $\alpha = 6\pi/3$ and ideally no fringe contrast would be seen. A finite atomic separation between the fault planes can result in faint fringes appearing as in the present case. Fig. 6b is a schematic drawing showing how systems of overlapping intrinsic faults could give rise to the fringe contrast observed in the fault complex.

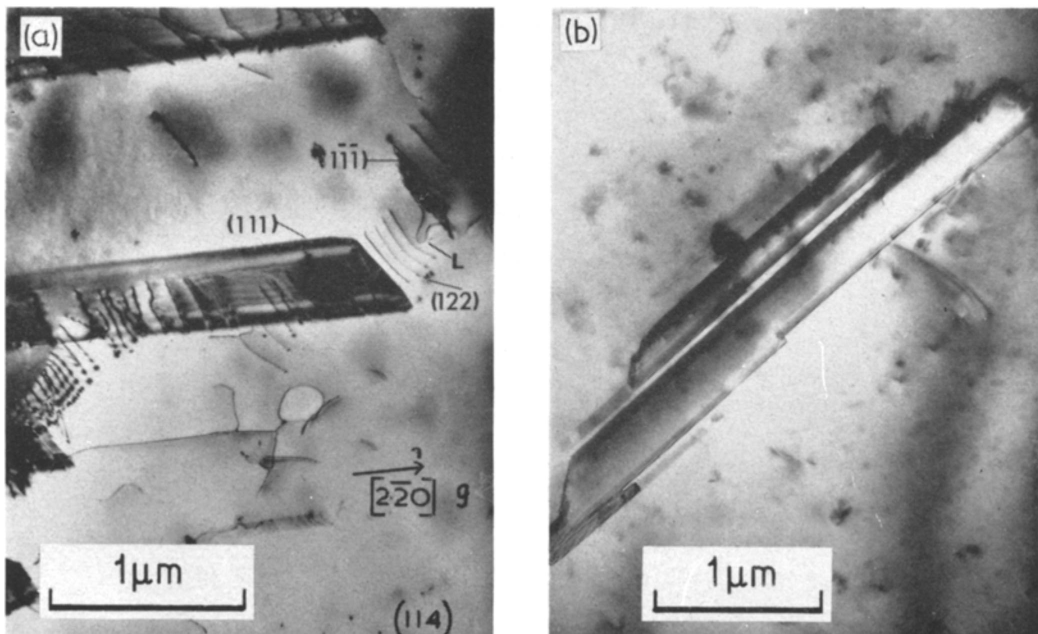

Figure 5 (a) Dislocations in a subgrain boundary in specimen AP136/7. The boundary planes as determined by trace analysis are indicated. A cross slip loop is marked L. (b) a microtwin present in a different area of the same specimen (multibeam reflection).

3.2. Pulled Material

Pulled material produced at SERL is mainly for use as substrate material for liquid phase epitaxy. In a device it provides electrical contact to the overgrown n+ layer and so must itself be n-type material with a high conductivity. In general the material is doped with Te or S to a free electron concentration of about 1×10^{18} cm^{-3}. The specimens subjected to examination are listed in table IV.

TABLE IV GaP specimens grown by Czochralski pulling from the melt using liquid encapsulation.

Specimen (SERL No.)	Doping	Free electron conc cm^{-3}
PEO 2	Undoped	—
PEO 77	S	9×10^{17}
PEO 53	S	1×10^{18}
PEO 78	S	1×10^{18}
PEO 73	S	2×10^{18}
PEO 24	Te	3×10^{17}
PEO 47	Te	1×10^{18}
PEO 48	Te	1×10^{18}

In the undoped specimen PEO 2, preferential attack occurred at planar defects during the thinning process. A number of these faults were analysed and all found to be intrinsic. Stacking fault tetrahedra were also found together with dislocations.

In all the sulphur doped material a dotted background was visible in the micrographs. The use of stereo pairs of micrographs showed these spots to be inside the material and not surface features. This was evidence of what could be precipitation. In specimen PEO 53 the spots were measured as about 40 Å diameter and appeared to show an interaction with the extinction contours. This would be consistent with them being precipitates, made visible by the structure factor contrast mechanism (Hirsch *et al* [21]). An order of magnitude estimate was made of the total volume of the precipitates shown in this micrograph. The average diameter of the precipitates was measured as near 40 Å and the density measured as five particles per 10^{-10} cm^2 area. The specimen thickness was estimated as 5000 Å and this gave a precipitate density of 1 part in 3×10^4 by volume. This is equivalent to about $1{\cdot}5 \times 10^{18}$ precipitate atoms/cc. which is of the right order ofmagnitude.

In the Te doped material little evidence of precipitation was found. In one specimen (PEO 48) a number of dark spots were observed and stereo pair analysis showed these to be in the material itself. Also present in this specimen was a dislocation with a single helical loop. Some precipitation was apparently associated with this defect.

3.3. GaP grown by Liquid Phase Epitaxy

GaP diodes were fabricated at SERL by a double epitaxial process using pulled material as the substrate. An n+ layer, doped with Te or S, was grown by liquid epitaxy on to the substrate and a p layer (Zn-O doped) was overgrown on to this. Some specimens were received with both the n+ and p layers and others with just the n+ layer (table V). Thinning of the specimens with Zn-O doped p-type layers was made difficult by the grooved and pitted nature of the surface. During thinning, holes formed first at the pits and the subsequent formation of a suitable thin area was only occasionally found possible. The depth of the pits was found to be too great to allow a suitably flat surface to be produced initially by mechanical polishing without danger of reaching the p-n junction. In general, the liquid epitaxial Te or S doped layers were found to be better and little difficulty was experienced in producing adequate thin areas. On the microscopic scale these n+ layers were found to be of good quality. No stacking faults or dislocations were observed in any specimen.

TABLE V Free charge carrier densities per cm^3 of liquid-epitaxial specimens examined in the electron microscope. All were grown on pulled GaP substrates and the n+ layers were doped with Te and the p layers with Zn-O.

Specimen (SERL No.)	p Layer	n+ layer
JN 162	—	1×10^{18}
JN 64	—	1×10^{18}
JN 151	—	1×10^{18}
JN 148	—	1×10^{18}
L 322	1×10^{18}	$2\text{-}4 \times 10^{18}$
L 222	1×10^{18}	$2\text{-}4 \times 10^{18}$
L 343	1×10^{18}	1×10^{18}
L 317	1×10^{18}	1×10^{18}

The Zn-O doped layers were, on the microscopic scale, found to be less perfect than the n+ layers. In all the specimens dislocations were observed. The overall dislocation density was estimated at about 4×10^6 cm^{-2}. Evidence of

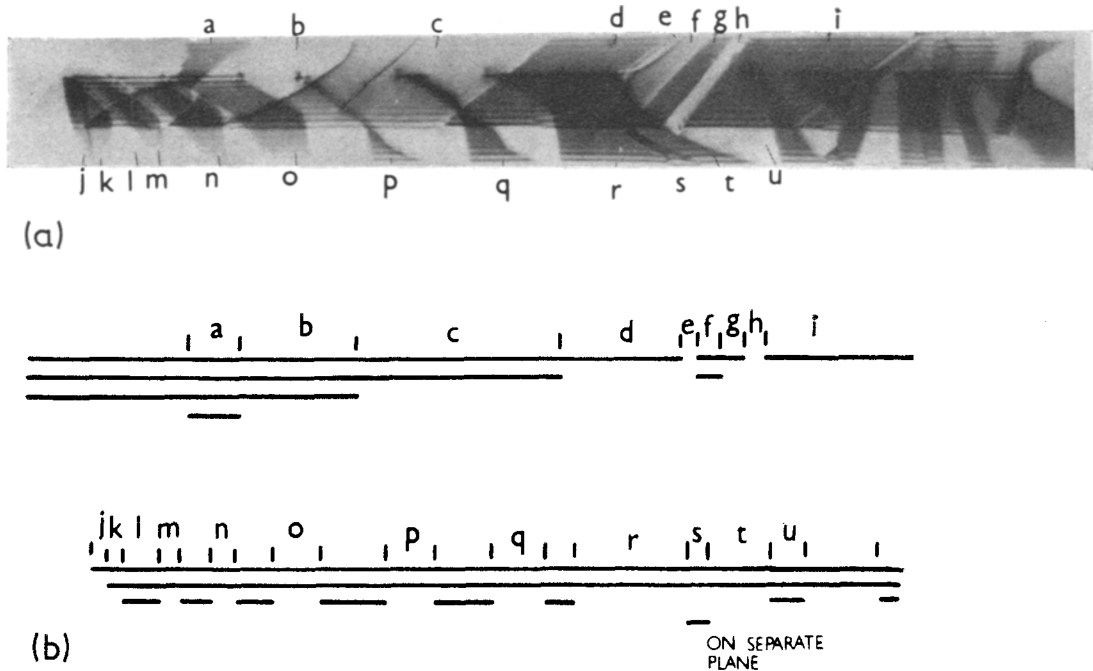

Figure 6 (a) Complex stacking fault structure in specimen no. AP118/2. (b) Diagram drawn looking parallel to the plane of the faults showing possible overlapping arrangements of single intrinsic faults to give rise to the observed contrast.

precipitation was also seen in the form of a number of isolated spots. As with the n+ layers no stacking faults were observed.

4. Discussion

4.1. Defects in Vapour Phase Grown GaP

Comparison of the electron microscope results for material grown by the three different basic processes shows that the heaviest concentrations of defects occur in material grown by vapour phase epitaxy. Typically the dislocation density in the vapour grown layers was between 10^7 and 10^8 cm^{-2} compared to densities of about 10^5 to 10^6 cm^{-2} in pulled material. In n-type liquid epitaxial layers the dislocation density was too low to be measured using the electron microscope but in the Zn-O doped material the density was estimated at about 10^6 cm^{-2}. Vapour phase material does not make efficient electroluminescent diodes and this may be because the defects introduce a large number of non-radiative centres into the material. It has been suggested that the origin of the dislocations in vapour phase grown material is attributable to the lattice and thermal expansion mismatch between GaP and the GaAs substrate [29, 30]. Abrahams *et al* [31] working with $GaAs_{1-x}P_x$ layers on GaAs found evidence that the principal factor was the lattice mismatch. They reported sets of inclined dislocations projecting upwards through the epitaxial layer and originating from the misfit dislocations at the interface. In the present work it was found that both the dislocation and stacking fault density increased with doping. The increased density of stacking faults that occur when the material is doped can be explained if the stacking fault energy is reduced by Suzuki segregation [32]. This is segregation of impurities either to or away from the fault so that the stacking fault energy γ is reduced resulting in an increase in the fault area by further separation of the bounding partials. It is also possible that due to the Suzuki effect a reduction in γ will occur on atomic planes closely adjacent to the stacking fault. Dislocations on these planes will then require less energy to dissociate into further stacking faults lying parallel to and overlapping the original fault. Examples of overlapping fault structures are clearly seen in figs. 3 and 6. The preferential etching effects observed in the vicinity of faults are consistent with a localised

increase in the concentration of impurity atoms.

In epitaxial layers of silicon, Booker [6] showed that stacking faults could arise from nucleation centres on the substrate and propagate through the layer. This generally resulted in the tetrahedral type of stacking fault although in some cases only one side of the fault tetrahedron was propagated. In vapour grown GaP the linear type of stacking fault was very common whereas only a few isolated faults of the tetrahedral variety were found. To explain the predominance of the linear type of fault there are two possibilities. Either only one side of tetrahedral faults nucleated at the substrate interface propagated through the layer or else the faults are formed independently by dissociation of dislocations. In either case Suzuki segregation would be influential. If the faults all initiated by the tetrahedron mechanism at the substrate interface and propagated through the epitaxial layer then the width of the faults at the surface of the layer should be the same. In general this was found not to be the case. Moreover the common occurrence of overlapping faults on neighbouring parallel planes is not readily explained by the tetrahedral fault mechanism. It is concluded that the majority of faults in this material were formed either by dissociation of dislocations or else possibly by nucleation at defects, such as precipitates, within the epitaxial layer.

Analysis of the dislocations associated with the faults in fig. 3 showed that the majority were Shockley partials but that in some cases the bounding dislocations were Frank partials. The presence of the latter suggests that stacking faults, lying for example in a (1 1 1) plane, may form by dislocation dissociation with the reaction

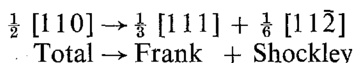

$$\tfrac{1}{2}\,[1\,1\,0] \rightarrow \tfrac{1}{3}\,[1\,1\,1] + \tfrac{1}{6}\,[1\,1\,\bar{2}]$$
$$\text{Total} \rightarrow \text{Frank} + \text{Shockley}$$

In this case the Frank partial will be sessile and any expansion of the fault will occur by motion of the Shockley partial. Faults bounded by two Shockley partials could also form by a reaction of the type:

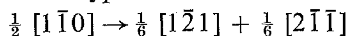

$$\tfrac{1}{2}\,[1\,\bar{1}\,0] \rightarrow \tfrac{1}{6}\,[1\,\bar{2}\,1] + \tfrac{1}{6}\,[2\,\bar{1}\,\bar{1}]$$

All the faults observed were intrinsic. This compares with the work of Abrahams and Tietjen [12] who observed intrinsic faults bounded by Shockley partials in $GaAs_{1-x}\,P_x$ alloys. Similarly in their work, faults were only observed when the epitaxial layers were doped.

4.2. Defects in Pulled and Liquid Epitaxial GaP

One of the objects of this examination was to try to establish the precise nature of the defects responsible for the difference in etching characteristics between pulled and liquid epitaxial GaP, and also why diodes formed by the growth of a single Zn-O doped layer directly on to a pulled n-type substrate are very inefficient. In general, the pulled material, etched using the procedure described by Saul [29], shows a number of characteristic dislocation etch pits. However, a much more dense array of smaller etch pits is also generally found to be present. These pits which do not occur in liquid epitaxial material are not fully explained. It was noted that defects in the pulled substrate did not appear to have grown into the epitaxial layer. The present electron microscope study did not detect any defects peculiar to the pulled material to which this etching characteristic might be attributed. One possible explanation is that the etching characteristics of pulled material are influenced by a lack of stoichiometry. This would not be detectable using the electron microscope if no clustering or ordering of the point defects occurred but could lead to changes in the chemical and physical properties of the material. In particular the presence of Ga vacancies might be expected to encourage the formation of the $V_{Ga} + Te_3$ type of complex described by Vieland and Kudman [33]. It is not possible to be specific as to whether Ga or P vacancies are likely to predominate in non-stoichiometric GaP. Little is known about the existence region of GaP. In any case the numbers of Ga and P vacancies would depend on the equilibrium established between the partial pressure of phosphorus vapour over the melt and the growing material. However, it is possible that this partial pressure may be increased due to the vapour being in contact with portions of the melt at temperatures much higher than the melting point and this could result in excess phosphorus being incorporated into the growing crystal. It has been found, in fact, that some Ga often remains in the crucible after the crystal has been pulled (S. J. Bass, SERL, Baldock, Herts, private communication). Ga vacancies, if present in the substrate, could act as sinks for Zn diffusion from the epitaxially grown Zn-O doped layer. It is possible that this could deplete the radiative centres of Zn and so lead to inefficient diodes. This interpretation would be

consistent also with the measurements of Calverley and Wight [34] and of the present authors [5] using scanning electron microscopy. These observations show that in the p-type material of poor diodes the Zn-O recombination centres within a few microns of the electrical p-n junction are generally of reduced efficiency. In the worst diodes, those grown by single epitaxy on pulled substrates, this inefficient region was up to 10 μm wide.

In layers grown by liquid epitaxy from a Ga melt, any stoichiometry variations will be on the Ga rich side of the existence region. Thus in a diode grown by double epitaxy, no excess of Ga vacancies is likely to be present near the p-n junction. The possible presence of excess P vacancies in this material may influence device efficiency but this has not yet been established.

The very low defect concentration found in GaP grown by liquid epitaxy is in accordance with the electroluminescent efficiencies found in this type of diode. Dislocation densities were low even at high doping levels. Precipitation may well be the limiting factor in determining the ratio of radiative to non-radiative centres which is critical for luminescent efficiency. Ladany [1] showed that diode efficiencies could be increased by optimisation of the amount of Zn and O added to the p melt. When excess dopants were added above this optimum, the efficiency of the diodes decreased. It is likely that this drop off in efficiency is due to the introduction of competing non-radiative centres possibly in the form of precipitates. It would appear from the evidence of the electron micrographs (sections 3·2 and 3·3) that precipitation, in the form of complexes the order of 40 Å in diameter, is present in all Te and S doped samples with free carrier concentrations near 1×10^{18} cm^{-3}. Some similar evidence of what may be precipitation was also found in Zn-O doped specimens. Precipitates of a comparable nature have been observed in n-type GaAs [8, 9, 35] and have been identified by electron diffraction and Moire fringe spacings to be of the Ga_2Se_3 and Ga_2Te_3 type. In the present work the precipitate density was too low to enable any positive identification to be made but it is likely that the precipitates are of a similar type. Precipitation in Zn-O doped GaP [36] and Zn diffused GaAs [3, 37] may not be comparable as the precipitates were much larger in size than those observed in the present work.

4.3. Defects and Diode Performance

A general correlation between diode efficiency and crystalline perfection thus emerges from the observations reported here. The vapour phase epitaxy material contained relatively high densities of intrinsic stacking faults and dislocations and at high doping densities there was evidence of precipitation. The defect density was found to increase with doping level indicating an interaction between impurities and imperfections. This material makes low efficiency diodes. Pulled material had an intermediate defect density but this alone was not enough to explain the poor quality of diodes grown by single epitaxy. The evidence suggests that deviation from stoichiometry and/or undesirable impurities may be important. Liquid epitaxy material was structurally the most perfect and makes the most efficient diodes. This correlation is in agreement with the general experience that the most perfect material makes the best semiconductor devices.

Acknowledgements

Thanks are due to Professor J. G. Ball for the provision of research facilities and to the Services Electronics Research Laboratory for the supply of material. This work was supported by a CVD contract and is published by permission of the Ministry of Defence.

References

1. I. LADANY, *J. Electrochem. Soc.* **116** (1969) 993.
2. I. LADANY, S. H. MCFARLANE, and S. J. BASS, *J. Appl. Phys.* **40** (1969) 4984.
3. M. J. HILL and D. B. HOLT, *J. Mater. Sci.* **3** (1968) 244.
4. D. B. HOLT and B. D. CHASE, *ibid* **3** (1968) 178.
5. *Idem, ibid* to be published.
6. G. R. BOOKER, *Disc. Faraday Soc.* **38** (1964) 298.
7. P. HAASEN and H. ALEXANDER, *Sol. State Phys.* **22** (1968) 27.
8. E. S. MEIRAN, *J. Appl. Phys.* **36** (1965) 2544.
9. M. S. ABRAHAMS, C. J. BUIOCCHI, and J. J. TIETJEN, *ibid* **38** (1967) 760.
10. M. S. ABRAHAMS and C. J. BUIOCCHI, *J. Phys. Chem. Sol.* **28** (1967) 927.
11. D. LAISTER and G. M. JENKINS, *J. Mater. Sci.* **3** (1968) 584.
12. M. S. ABRAHAMS and J. J. TIETJEN, *J. Phys. Chem. Sol.* **30** (1969) 2491.
13. D. LAISTER and G. M. JENKINS, *J. Mater. Sci.* **5** (1970) 862.
14. M. J. HILL, D. B. HOLT, and B. A. UNVALA, *J. Sci. Instrum.* **1** (1968) 301.

15. C. S. FULLER and H. W. ALLISON, *J. Electrochem. Soc.* **109** (1962) 880.
16. B. D. CHASE, D. B. HOLT, and B. A. UNVALA, *J. Electrochem. Soc.* (1972) to be published.
17. B. D. CHASE, D. B. HOLT, J *Electrochem. Soc.* (1972) to be published.
18. S. J. BASS and P. E. OLIVER, *J. Cryst. Growth* **3** (1968) 286.
19. R. C. TAYLOR, J. F. WOODS, and M. R. LORENZ, *J. Appl. Phys.* **39** (1968) 5404.
20. S. AMELINCKX, *Sol. State Phys. Suppl.* **6** (1964), "The Direct Observation of Dislocations (Academic Press, New York).
21. P. B. HIRSCH, A. HOWIE, D. W. PASHLEY, M. J. WHELAN, and R. B. NICHOLSON, "Electron Microscopy of Thin Crystals" (Butterworths, London, 1965).
22. J. HORNSTRA, *J. Phys. Chem. Solids* **5** (1958) 129-141.
23. D. B. HOLT, *ibid* (1962) 1353.
24. J. M. SILCOCK and W. J. TUNSTALL, *Phil. Mag.* **10** (1964) 361.
25. A. HOWIE and M. J. WHELAN, *Proc. Roy. Soc.* **A.267** (1962) 206.
26. B. D. CULLITY, "Elements of X-ray Diffraction" (Addison Wesley, Reading, 1956).
27. G. GEISEKE, in "Semiconductors and Semimetals" (eds. R. K. Willardson and A. C. Beer) (Academic Press, New York, 1966) **2** 63.
28. M. J. WHELAN and P. B. HIRSCH, *Phil. Mag.* **2** (1957) 1121 and 1303.
29. R. H. SAUL, *J. Electrochem. Soc.* **115** (1968) 1184.
30. *Idem, J. Appl. Phys.* **40** (1969) 3273.
31. M. S. ABRAHAMS, L. R. WEISBERG, C. J. BUIOCCHI, and J. BLANC, *J. Mater. Sci.* **4** (1969) 223.
32. H. SUZUKI, in "Dislocations and Mechanical Properties of Crystals" (Eds. J. C. Fisher, W. G. Johnston, R. Thomson, and T. Vreeland) (Wiley, New York, 1957) p. 361-388.
33. L. J. VIELAND and I. KUDMAN, *J. Phys. Chem. Solids* **24** (1963) 437.
34. A. CALVERLEY and D. R. WIGHT, *Sol. State. Electron.* **13** (1970) 382.
35. H. KRESSEL, F. Z. HAWRYLO, M. S. ABRAHAMS, and C. J. BUIOCCHI, *J. Appl. Phys.* **39** (1968) 5139.
36. M. GERSHENZON and R. M. MIKULYAK, *ibid* **35** (1964) 2132.
37. J. F. BLACK and E. D. JUNGBLUTH, *J. Electrochem. Soc.* **114** (1967) 188.

Received 7 April and accepted 24 September 1971.